An Active Microwave Limb Sounder for Profiling Water Vapor, Ozone, Temperature, Geopotential of Pressure Surfaces and Clouds

E. R. Kursinski, D. Flittner, B. Herman, D. Feng, S. Syndergaard, D.Ward
Department of Atmospheric Sciences
The University of Arizona
Tucson, AZ 85721-0081

***Abstract* - We present and characterize the performance of a new remote sensing concept extrapolated from the GPS occultation concept in which we choose the signal frequencies to determine profiles of atmospheric water, ozone, temperature, geopotential of atmospheric pressure surfaces and clouds.**

I. Introduction

Our continual quest towards a deeper understanding of weather and climate and a significantly improved skill to predict their future behavior depends critically on our knowledge of the present structure of the atmosphere and its variations. Here we present and discuss a particular implementation of the spacecraft radio occultation technique designed to characterize the thermodynamic and compositional structure if the atmosphere. We have referred to this concept by several names depending on our emphasis. The Active Tropospheric Ozone and Moisture Sounder (ATOMS) is an ongoing Instrument Incubator Program (IIP). We have also used the acronym, Active Limb-viewing Spectrometry by Occultation (ALSO) to make the point that constituents can be characterized by occultation when the occultation signal frequencies are selectable. In the present context, we will use the acronym, BRIGHTOC, standing for Bi-static Radar Imaging of Geopotential, Humidity, Temperature, Ozone and Clouds, similar to the acronym used by *Kursinski et al.* (2002). We will summarize the results of *Kursinski et al.* (2002) who focused primarily on clear sky conditions and then extend the analysis to evaluate and illustrate the capabilities of these observations in cloudy conditions.

II. Background

The spacecraft radio occultation technique has proven quite powerful in characterizing the major planetary atmospheres of our solar system including that of Earth. In this technique one or more monochromatic signals are transmitted from a spacecraft across the planet's limb to a receiver on the far side of the limb (see Figure 1). Since the transmitters and receivers are independent, the system is referred to as "bi-static" radar. The orbital motion of the transmitter and receiver cause the signal path to slice down through the atmosphere providing a vertical limb scan of the atmosphere. These observations provide a unique combination of dynamic range, accuracy, high vertical resolution, all-weather sensing and global coverage.

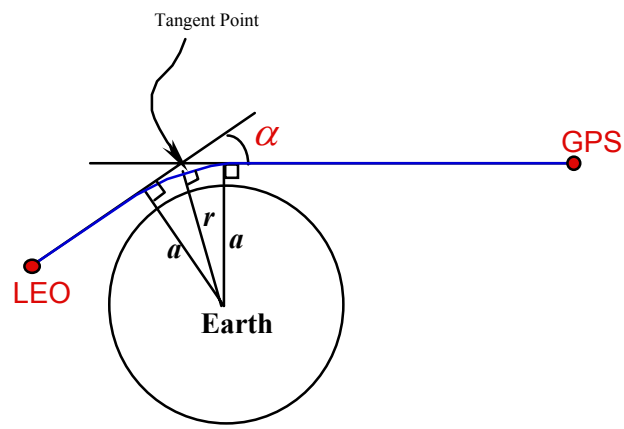

Fig. 1. Satellite to satellite occultation geometry.

Historically, radio occultation observations have utilized pre-existing spacecraft signals such as the occultation observations of the outer planets using Voyager's telecommunications signals (*Tyler et al.*, 1989) or the observations of Earth's atmosphere using signals from the Global Positioning System (GPS) satellites (*Ware et al.*, 1996; *Kursinski et al.*, 1996). In the present work, we describe what could be accomplished if we were to choose the occultation signal frequencies and develop the associated instrumentation.

In Earth's atmosphere at frequencies less than 300 GHz, refractivity, defined as $N = (n\text{-}1) \times 10^6$ where n is the index of refraction, is related to temperature (T), total pressure (P_t) and partial pressure of water (e) as

$$N = 77.6\,(P_t/T) + 3.73\times10^5\,(e/T^2) \qquad (1)$$

In the GPS case, very accurate profiles of the atmospheric refractivity are derived which lead directly to density, pressure and temperature in the upper troposphere through the stratosphere because the contribution of moisture to (1) is negligible at these altitudes. In the lower half of Earth's troposphere, water vapor contributes significantly to the index of refraction such that additional information such as temperature from a weather analysis is required to determine the wet and dry contributions to the index of refraction. Given present knowledge of atmospheric temperature to roughly 1.5 K, one can derive moisture from GPS occultations to an accuracy of roughly 0.1-0.2 g/kg, which is useful in the lower to middle troposphere (*Kursinski et al.*, 1995; *Healy and Eyre*, 2000; *Kursinski and Hajj*, 2001). The

approach of combining temperature with the GPS-derived refractivity to determine moisture is suboptimal in that it essentially assumes the temperatures are known perfectly, which of course is incorrect. A more optimal approach combines the GPS observations with weather analysis estimates of temperature, pressure and moisture in a least squares framework based on the respective error covariances of the observations and the analysis. Such least squares schemes are under development (*eg. Zou et al*., 1999; *Healy and Eyre*, 2000; *Kursinski et al*, 2000a, b; *Poli et al.,* 2002). While quite powerful, we would like an observational system that directly provides profiles of moisture and temperature independent of models with the accuracy and vertical resolution of the GPS refractivity profiles.

Spacecraft radio occultations (such as those using GPS) have generally focused on deriving bending angle profiles from the changing Doppler shift during an occultation which is derived from measurements of the carrier phase. (For a detailed description of the GPS occultation technique, resolution, and theoretical accuracy, see *Kursinski et al*., 1997.) In such cases, the index of refraction, n, is taken to be real. However, n is in general complex, n_c, because a medium will affect both the speed of propagation and the amplitude of signals via absorption as they pass through it. The information in n_c is contained in the refractivity, N_c, the non-unity portion of n_c defined such that $N_c = (n_c - 1)\text{x}10^6$. N_c is also complex having real (N') and imaginary (N'') parts such that $N_c = N' + \text{i}N''$. Knowing profiles of both N' and N'' provides the constraints to solve for profiles of moisture concentration, temperature and pressure. Spacecraft radio occultation observations have inferred ammonia concentrations in the outer planets (*Lindal et al*., 1981) and H_2SO_4 concentrations in the atmosphere of Venus (*Jenkins and Steffes*, 1991; *Jenkins et al*., 1994) by utilizing absorption measurements. In the rest of the paper, for simplicity, we will write $N = N'$ as representing the real part of N_c as was done in (1).

The BRIGHTOC system described here would measure the phase and amplitude of several monochromatic signals near the 22 and 183 GHz water lines and 195 GHz ozone line as they pass through the atmosphere during an occultation. From the measured phase and amplitude, we can derive profiles of both the speed of propagation and the attenuation due to water absorption and in turn solve for the wet and dry density profiles directly from the occultation observations. Because we control the signal source characteristics, BRIGHTOC provides very high signal-to-noise ratios (SNR). The vertical resolution of the technique is limited by Fresnel diffraction rather than aperture diffraction which ultimately limits passive observations. Figure 2 shows the vertical resolution at different wavelengths as a function of altitude. The result is a high vertical resolution, all-weather active limb-sounder yielding very precise and accurate moisture, temperature and geopotential profiles from the surface to the mesopause as well as liquid and ice clouds and profiles of other constituents such as ozone.

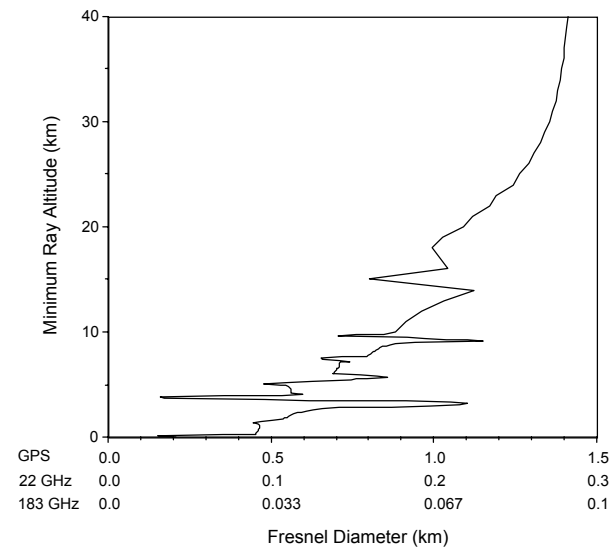

Fig. 2: Diffraction limited occultation vertical resolution at 1.6, 22 and 183 GHz.(from Kursinski et al., 2002)

III. Inversion Theory: Retrieving Atmospheric Structure from Amplitude

A. Conversion of Occultation Absorption Profiles into Profiles of Absorption Coefficients

Signal intensity, I, is reduced by absorption along the signal path as

$$dI = -I\ k\ dl$$

where k (= $4\pi N''/\lambda_0$ x10^{-6}) is the extinction coefficient, l is distance along the signal path and λ_0 is the signal wavelength in a vacuum. For each wavelength, the observed intensity, I, is related to the vacuum intensity, I_0 (the signal intensity with no atmosphere), as $I = I_0\ e^{-\tau}$ where τ is the optical depth integrated along the signal path through the atmosphere. Therefore τ is determined from the intensity according to (2)

$$\tau = \ln(I_0/I) \qquad (2)$$

While the measured optical depth is integrated along the occultation signal path, the desired quantity is the radial profile of the extinction coefficient, k. Given k and N as functions of r, the distance from the center of curvature (approximately the center of the Earth), we can derive a radial profile of atmospheric water. Under the assumption of local spherical symmetry, the optical depth and extinction coefficient are related by an abel transform pair, (3) and (4), analogous to the standard bending angle and index of refraction transform relation derived by *Fjeldbo et al.* (1971).

$$\tau = \int k dl = \int_{r_0}^{\infty} k \frac{n\ r\ dr}{\left(n^2 r^2 - n_0^2 r_0^2\right)^{1/2}} \qquad (3)$$

$$k = -\frac{1}{2\pi}\frac{da}{dr}\bigg|_{a=a_0}\int_{a_0}^{\infty}\frac{d\tau}{da}\frac{da}{\left(a^2-a_0^2\right)^{1/2}} \qquad (4)$$

(3) represents the forward problem of the extinction coefficient integrated along the occultation path. (4) is the inverse relation allowing us to derive the extinction coefficient profile from the measured, path-integrated optical depth. (4) can be derived from (3) via standard abel integral transform pair relations (*Tricomi*, 1985**;** *Feng et al*., 2001). Note that the independent variable in (4) is a, the asymptotic miss distance (see Figure 1) defined as $a = n\ r \sin\theta$ where θ is the angle between the ray path and radial direction. a is a constant for each ray path under the assumption of spherical symmetry and is derived from the atmospheric Doppler profile as described in Kursinski et al. (1997). k is then derived as a function of r in (4) using the fact that $a_0 = r_0\, n(r_0)$ where r_0 is the tangent radius of the raypath such that θ is $\pi/2$ and $n(r_0)$ is derived from the bending angle profile via the standard abel equation.

B. Use of on-line and off-line tones to remove unwanted effects

To remove noise and provide dynamic range, profiles of optical depth will be measured at several frequencies. We will then ratio the amplitudes of signals with similar frequencies to eliminate unwanted common noise and atmospheric effects. Therefore the optical depth used in (3) will actually be the difference between the optical depths measured at 2 different frequencies,

$$\tau_{12} = \tau_1 - \tau_2 = \ln\left(\frac{I_{10}}{I_1}\frac{I_2}{I_{20}}\right)$$

where the subscripts, 1 and 2, refer to two frequencies, f_1 and f_2. The resulting extinction coefficient profile derived from (4) will be $k_1 - k_2$.

A point worth emphasizing is the *absolute* signal amplitude is not relevant. Rather, it is the variations in amplitude that occur during an occultation that are the signatures of interest. The signal amplitudes will be normalized to the amplitude observed immediately before or after each occultation when the signal path is entirely above the atmosphere. The amplitude normalization of every occultation will eliminate long-term drifts yielding a technique extremely well suited for observing long-term climate variations.

C. Conversion of Absorption Coefficients and Refractivity into Temperature, Pressure, Water Vapor & Cloud Liquid

In the upper troposphere and stratosphere, where there is no liquid water, we have profiles of two observables, $k_1(r)$-$k_2(r)$ and $N(r)$, from which can derive temperature (T), total pressure (P_t) and partial pressure of water vapor (e) by simultaneously solving 3 equations, the refractivity equation, (1), the absorption equation, (5), and the hydrostatic equation.

$$k_1(r) - k_2(r) = F(f_1, f_2, P_t, e, T) \qquad (5)$$

f_1 is positioned on the line to measure absorption and f_2 is positioned off-line to calibrate out unwanted effects. The absorption coefficient which includes individual lines as well as the water vapor continuum is a strong function of e and weaker function of P_t and T, and therefore constrains primarily e. P_t and T determine the line shape and the absorption due to O_2.

Since the hydrostatic relation is a differential equation we need a boundary condition to initialize the hydrostatic integral such as temperature in the upper mesosphere. By measuring N and k at several frequencies to provide the dynamic range needed to sense water throughout the troposphere and middle atmosphere, the observations provide additional constraints. At altitude intervals where two different pairs of frequencies each provide independent estimates of the extinction coefficients and therefore e, P_t, and T, the overlapping constraints provide the information needed to determine the hydrostatic boundary condition.

In the lower troposphere, we must solve for the liquid water, C_l, along the path as well. We therefore must measure the occultation signal intensity at an additional frequency. We will then take the 3 observables, $k_1(r)$- $k_2(r)$, $k_2(r)$-$k_3(r)$ and $N(r)$ and simultaneously solve (1), (6a), (6b) and the hydrostatic equation.

$$k_1(r) - k_2(r) = F(f_1, f_2, P_t, e, T, C_l) \qquad (6a)$$

$$k_2(r) - k_3(r) = F(f_2, f_3, P_t, e, T, C_l) \qquad (6b)$$

Another pair of frequencies is required to characterize ozone.

$$k_4(r) - k_5(r) = F(f_4, f_5, P_t, [O_3], T, C_l) \qquad (7)$$

IV. Clear Sky Results

A. Ozone

Estimating the errors and accuracies of the technique require some combination of simulated retrievals and error covariance studies. We have used a combination of both. For ozone we have used used primarily retrieval simulations. Figure 3 shows occultation profiling can characterize ozone with approximately 1% precision through the stratosphere down to approximately 8 km altitude. At lower altitudes, the errors grow rapidly because the tropospheric ozone concentrations are significantly lower than the stratospheric concentrations.

B. Clear Sky Water, Temperature and Geopotential Accuracies

We now discuss the accuracies of retrieved water, temperature and geopotential for clear sky conditions based

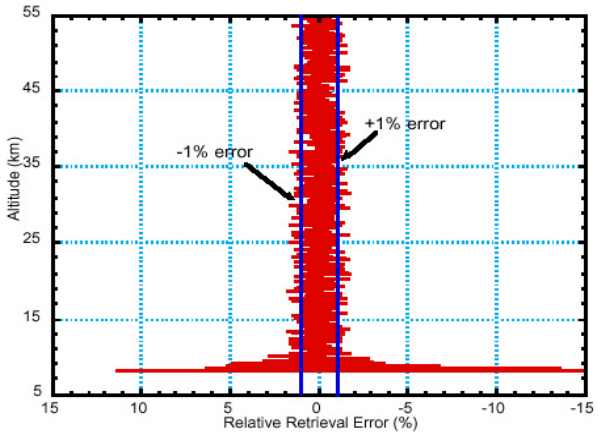

Fig. 3 - Percentage errors in a retrieved ozone profile at 195 GHz (from Feng et al., 2001)

on covariance results. We have a vector of observations, y, from an occultation profile from which we want to derive the atmospheric state vector, x, consisting of the atmospheric variables of interest: water vapor, temperature and surface pressure. Assuming a linear set of equations relate y and x, the statistically optimal weighted least squares solution for x is

$$x = \left[K^T S_y^{-1} K\right]^{-1} K^T S_Y y \qquad (8)$$

where K represents the gradient of y with respect to x and S_y is the observation error covariance. The error covariance, S_x, of x is

$$S_x = \left[K^T S_y^{-1} K\right]^{-1} \qquad (9)$$

While (1) and (5) are somewhat nonlinear, the fractional observational errors are quite small and (9) provides a representative estimate of the error in x resulting from errors in y (*Rodgers*, 1990).

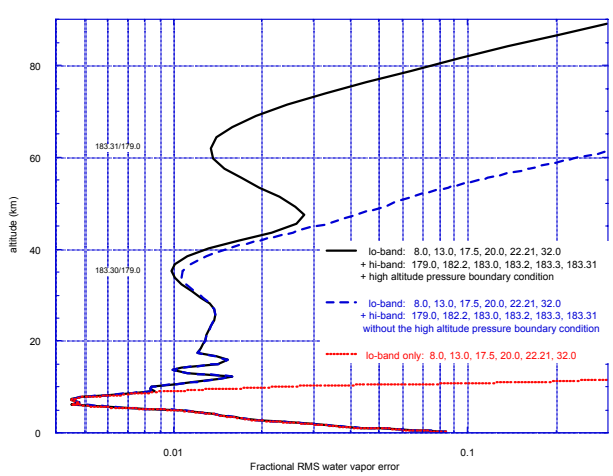

Fig. 4: Fractional water vapor error for tropical clear sky conditions (from Kursinski et al., 2002)

As Figure 4 shows, a combined 22 and 183 GHz occultation system can profile water vapor to ~1-2% or better precision from near the surface to 70 km altitude in clear conditions. The frequencies of the occultation tones are given in the Figure and Table I. Table I also summarizes critical features of the occultation links to achieve the very high SNR's required to achieve the precisions shown in Fig. 4. The Figure 4 results are for 250 m vertical resolution in the lower half of the troposphere, 500 m resolution in the upper troposphere and lower stratosphere and 1 km resolution in the stratosphere.

TABLE I
SUMMARY OF INSTRUMENT PERFORMANCE PARAMETERS USED IN ERROR COVARIANCE STUDY.

Frequency (GHz)	Radiated Power (W)	System Noise Temperature (K)	SNR_{v0}
8.0	12	150	4710
13.0	7	150	5840
17.5	6	150	7280
20.0	6	150	8320
22.21	6	150	9240
32.0	6	150	13300
179.	0.02	1500	1860
182.2	0.02	1500	1900
183.0	0.02	1500	1900
183.2	0.02	1500	1900
183.3	0.02	1500	1900
183.31	0.02	1500	1900

Loss was assumed to be 3 dB at each frequency. The antenna diameter was 30 cm for each frequency.

Figure 5a shows BRIGHTOC will profile temperature to a few tenths of a Kelvin precision. Figure 5b shows that BRIGHTOC can remotely determine the geopotential height of pressure surfaces to ~10 m. Combining the moisture and temperature information will yield relative humidity profile precisions of a few percent. Significantly better accuracies will be achieved when profiles are averaged to characterize climatological behavior.

The dashed line on the right hand side toward the center of Figures 4, 5a and 5b indicates the accuracy that can be achieved without initializing the hydrostatic integral at a high altitude. The figures show that below 40 km altitude, the pressure dependence of the absorption lines is sufficient to solve for the pressure directly without the high altitude hydrostatic integral initialization. Extending the high accuracy moisture, temperature and geopotential heights well into the mesosphere and above requires initialization of the hydrostatic integral at 90 km or above.

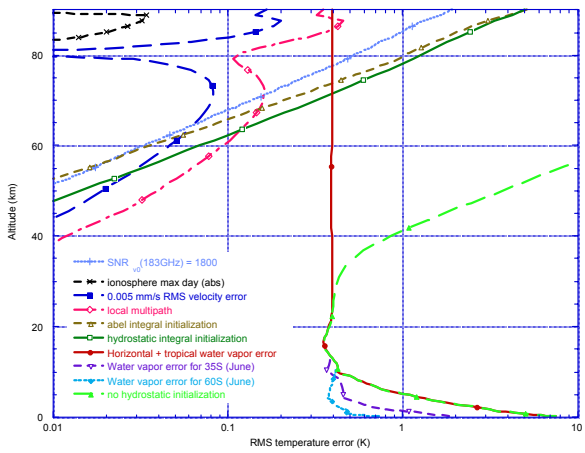

Fig. 5a: Temperature errors (from Kursinski et al., 2002)

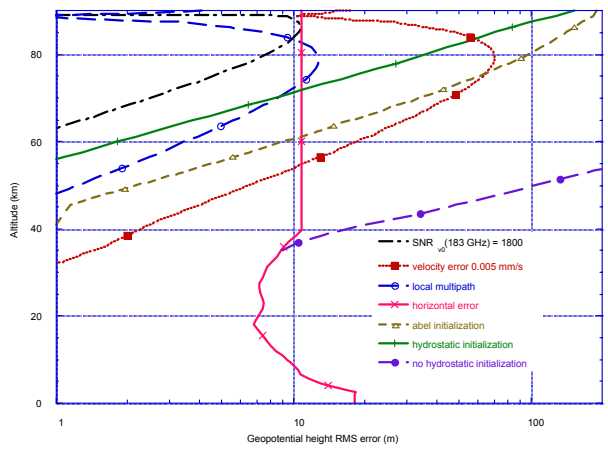

Figure 5b: Geopotential height errors (from Kursinski et al., 2002)

C. Improving the moisture estimates under high latitude winter conditions

Figure 4 shows that the 22 GHz occultation information (indicated as "lo-band only") extends from the surface to about 10 km altitude under low latitude conditions. Figure 6 shows that under high latitude winter conditions (60S in winter), the 22 GHz line information is limited to the lowest 4-5 km of the atmosphere because of the much smaller moisture abundances (see the dashed-dotted line in Figure 6). Use of the 183 GHz line is crucial to characterizing moisture above 3.5 km altitude under these cold, dry conditions (see solid line in Figure 6). Utilization of tones at 176 (dotted line) and 165 and 176 GHz (dashed line) can substantially improve moisture retrieval accuracy between 2 and 4 km altitude by probing the 183 GHz line farther from the line center to compensate for the increased pressure broadening at lower altitudes.

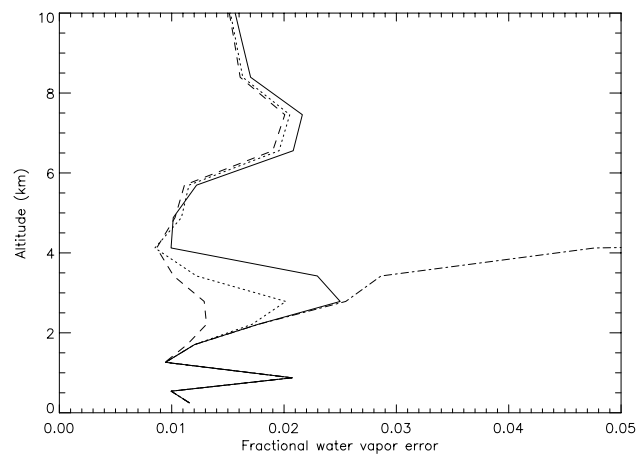

Figure 6: Water vapor error under high latitude winter conditions

V. Results in the Presence of Clouds

A. Liquid water impact on frequencies near the 22 GHz line

Liquid water absorbs at microwave frequencies. Therefore, when clouds are present, we must solve for liquid water in addition to water vapor, temperature and pressure. This affects our choice of frequencies near the 22 GHz line. It does not affect our choice of tones near the 183 GHz much because the 183 GHz line is used at altitudes where there is very little water which tend to be below freezing. As discussed in Section III.C we will have require at least one frequency beyond what we require in clear sky conditions.

B. Tropical liquid water cloud at 4 km

Figure 7 shows a simple liquid water cloud at 4 km altitude for tropical conditions.

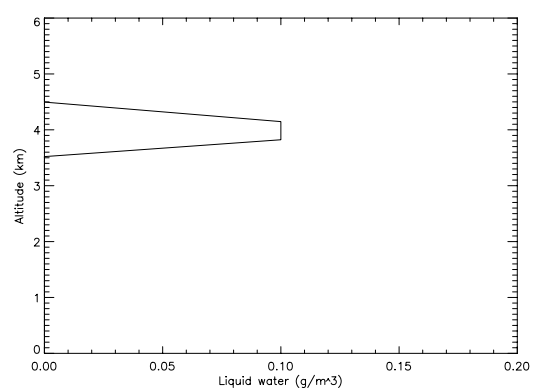

Figure 7: Liquid water profile for cloud near 4 km under tropical conditions

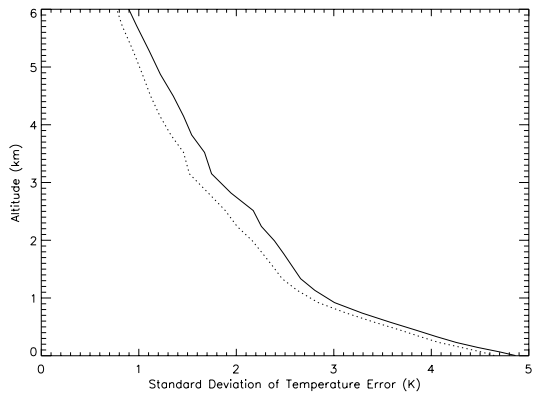

Fig. 8a. Temperature errors

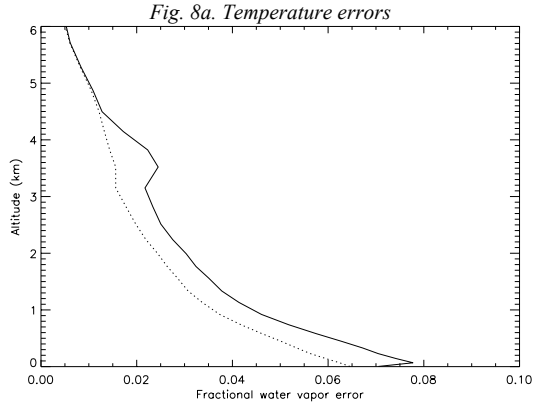

Fig. 8b. Water vapor errors

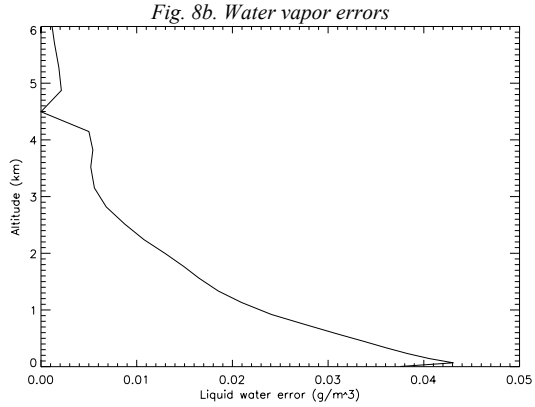

Fig. 8c. Liquid water errors

Figures 8a, 8b and 8c show the errors in retrieved temperature, water vapor and cloud liquid water. The dotted line in each retrieval is the clear sky retrieval in the absence of the cloud. The solid line in each figure is the full retrieval when the cloud is present. It is apparent that there is little degradation in the temperature and water vapor retrieval errors in the cloud case relative to the clear case. The cloud liquid water errors increase near the surface reaching a maximum of ~0.045 g/m^3. The cloud liquid water errors at the altitude of the cloud are ~0.005 g/m^3 amounting to a fractional error of 5% at the level of the cloud.

C. Marine stratus case

Marine stratus clouds such as exist off the coast of Southern California are an important component of Earth's climate system, particularly as a variable contributor to albedo. Because of their remote location, routine characterization of these clouds must be done via remote sensing. However, distinguishing between these clouds and the surface and characterizing these clouds presents a serious remote sensing challenge because of their low altitude. Microwave occultation observations are well suited to characterizing the marine boundary layer because of its lack of topography and general horizontal homogeneity. As a result, microwave occultation observations will characterize the vertical structure of marine stratus clouds far better than passive nadir viewing observations because of their high vertical resolution and ability to penetrate the clouds.

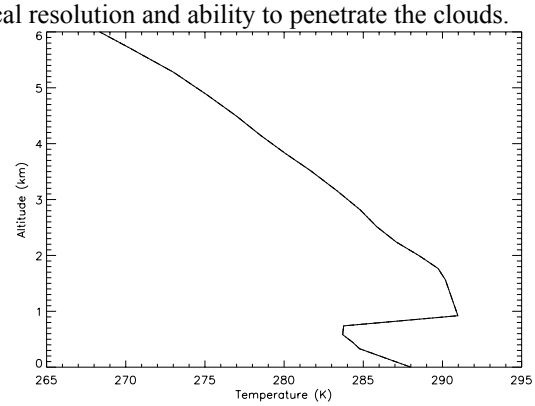

Fig. 9a. Marine stratus case temperature profile

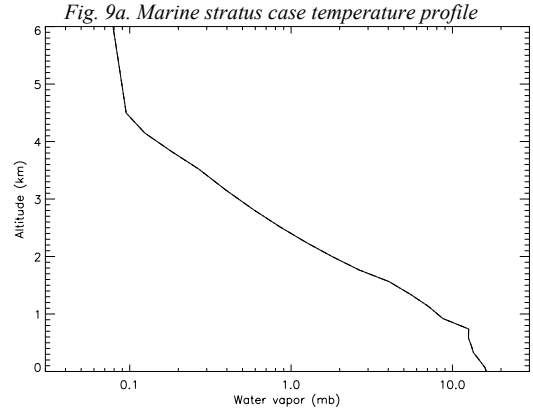

Fig. 9b. Marine stratus case water vapor profile

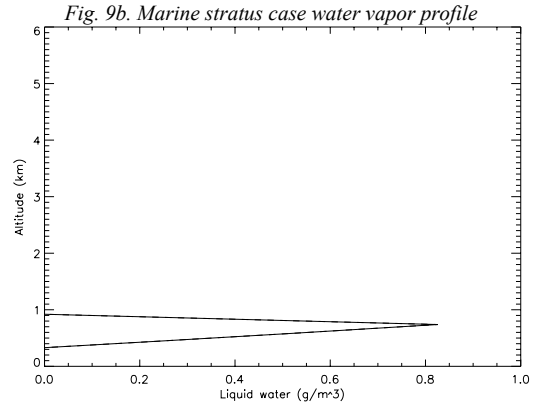

Fig. 9c. Marine stratus case liquid water profile

Figures 9a, 9b and 9c show the temperature, water vapor and liquid water profiles of marine stratus cloud deck case

based on dropsonde measurements of the coast of southern California from the DYCOMS II field campaign (*Stevens et al.,* 2002). The liquid water profile is that of a rather thick marine stratus deck with a peak liquid water density of 0.8 g/m^3 near 800 m altitude.

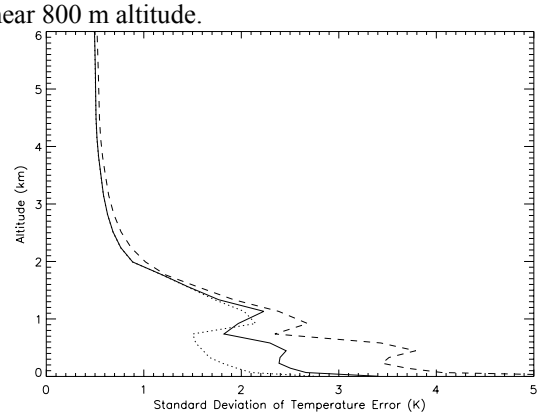

Fig. 10a. Temperature errors

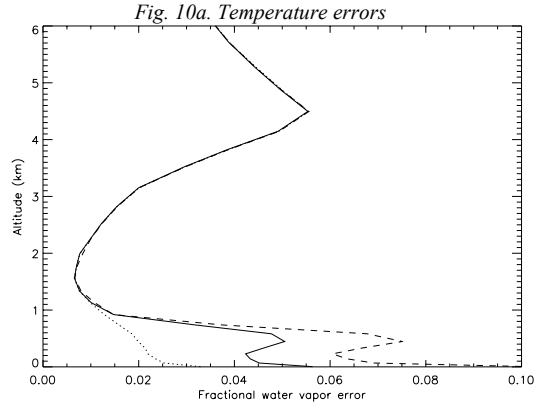

Fig. 10b. Water vapor errors

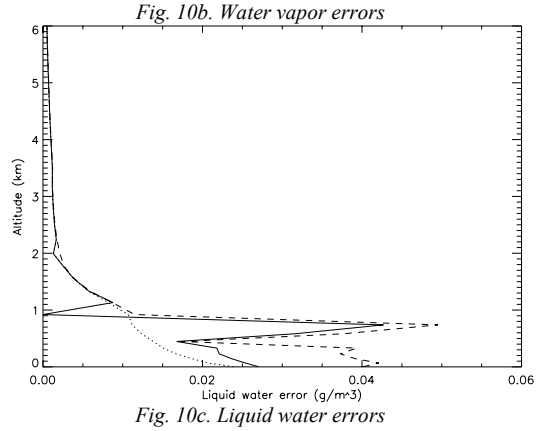

Fig. 10c. Liquid water errors

Figures 10a, 10b and 10c show the errors in retrieved temperature, water vapor and liquid water respectively for the Figure 9 case. The dotted line in each of the Figure 10 panels shows the error when we attempt to solve for liquid water but no cloud is present. This establishes a noise floor to the retrievals when clouds may be present. The solid line in each of the Figure 10 panels represents the error when the cloud is present and the amplitude of the 8 GHz frequency tone has been used to constrain the abundance of molecular oxygen and therefore the temperature of the bulk gas. *Kursinski et al.* (2002) showed that utilizing a low frequency tone to measure absorption by the 60 GHz O_2 feature significantly reduces errors in the lowermost troposphere under warm and wet conditions. Under these conditions, the *k* and *N* constraints become almost redundant and an additional independent piece of information is required to separate the water and temperature effects. Sensing absorption by the 60 GHz feature provides a constraint on the O_2 number density and therefore temperature. The dashed line in each of the Figure 10 panels shows the temperature error when the 8 GHz tone is not used to constrain the O_2 abundance.

As shown in Figure 10a, the temperature error is less than 1 K above 2 km altitude in all cases. Below 1.5 km altitude the temperature error depends on the conditions. When no cloud is present, the temperature error is 2K or less. When the cloud in Figure 9c is present and we use the 8 GHz O_2 absorption constraint, the error within 1.5 km of the surface is 2 to 2.5 K and rises to ~3 K right at the surface. This amounts to about a 0.5 K degradation relative to the no cloud case. When we do not use the O_2 absorption constraint, the near-surface temperature error is 2.5 to 3.5 K rising to more than 4 K right at the surface.

Figure 10b show the fractional error in derived water vapor. Using the 8 GHz O_2 constraint yields errors 4 to 5% in the lowest km. The clear sky errors near the surface are 1 to 2%. Not using the O_2 absorption constraint yields errors of 6 to 8% within 1 km of the surface. The peak error near 4.5 km altitude can be reduced from about 5.5% shown in Figure 9b to about 3.3% using the 165 and 176 GHz signals similar to Figure 6.

Figure 10c shows the errors in the retrieved liquid water profile. Errors when solving for liquid water when none is present (dotted line) are 0.01 g/m^3 near 1 km altitude and increase to 0.02 g/m^3 at the surface. Above 2 km altitude errors are 0.002 g/m^3 or less. The errors when the cloud is present and the 8 GHz O_2 constraint is used (solid line) reach a peak of 0.04 g/m^3 at the cloud peak amounting to a fraction liquid water error of ~ 5%. The errors in the well mixed layer under the cloud are ~0.015 to 0.02 g/m^3. Above the cloud, the errors are essentially those when no cloud is present. The liquid water errors without the O_2 constraint are somewhat worse reach a maximum of 0.05 g/m^3 near cloud top and 0.04 g/m^3 below the cloud.

The results in Figure 10 reveal the potential for BRIGHTOC system to characterize the marine boundary layer to high accuracy and vertical resolution in clear conditions and when marine stratus clouds are present.

D. The impact of ice clouds

The occultation tones near 183 GHz will be sensitive to scattering by ice particles (e.g. Evans and Stephens, 1995). However, contamination by ice above the freezing level should not be a problem because the scattering effects are quite broadband, on-line/off-line ratioing described in Section III will remove almost most of the sensitivity (Kursinski et

al., 2002). We can sense the ice by examining attenuation profile of individual tones. We can obtain information on ice amount and attributes examining at least 2 tones widely spaced in frequency. We may use passive system to get wider frequency spacing than can be accomplished actively. Use of polarization may help sort out ice particle properties and orientations. The combined 22 and 183 GHz sensitivities may allow BRIGHTOC to characterize the combination of liquid and ice particles known to exist between 0 and –40°C, a poorly understood and characterized regime of behavior. Characterization of ice clouds by BRIGHTOC needs further examination but appears promising.

VI. Other Sources of Error

A. Horizontal errors

The errors we have described here have ignored horizontal variations in the atmospheric structure. To evaluate the impact of horizontal structure, we have examined the accuracy of occultation retrievals in the vicinity of fronts that represent a rather severe set of horizontal conditions encountered in Earth's atmosphere. It is important to recognize that occultation observations are not point measurements and therefore should not be evaluated as such. For a frontal surface oriented approximately orthogonal to an occultation plane, differences between the occultation derived moisture and the moisture at the ray path tangent point can be greater than 20%. However, when the occultation-derived moisture is compared with a weighted average along the ray path, the moisture "error" is 5% or less. If the frontal plane is oriented parallel to the occultation ray paths, the moisture errors are no more than 3% and generally a few tenths of a percent or less. Temperature errors are generally less than 1 K for ray path tangent point comparisons and about a factor of 5 less for comparisons with a weighted average along the ray path. Therefore, the 0.5 to 3% moisture errors described due to finite measurement SNR and residual diffraction effects here are quite relevant even under the rather severe horizontal conditions of fronts.

B. On-orbit spectroscopic calibration

The accuracies which BRIGHTOC appears capable of achieving are likely to push our spectroscopic knowledge of the absorption spectra of Earth's atmosphere. To address this issue, the BRIGHTOC tones will be tunable such that we can we can oversample the line shape and spectrum and solve for the absorption line parameters while in orbit.

VII. Summary and Conclusions

Using frequencies near the 22 and 183 GHz water lines and the 195 GHz ozone line, we can derive not only the speed of light as a GPS occultation does but also profiles of absorption caused by atmospheric water and ozone. Given the water information, we separate and solve for moisture, temperature, geopotential of pressure surfaces and cloud profiles. Clear sky error covariance results indicate the precisions of individual water profiles will be 0.5 to 3% extending from roughly 1 km to 75 km altitude. Ozone retrievals will have similar precisions in the upper troposphere and the stratosphere. Profiles of other atmospheric constituents can be derived using frequencies near strong lines of that constituent. Temperature accuracies of individual profiles will be sub-kelvin from ~1 km to 70 km altitude depending on latitude and season. Accuracies of geopotential heights of pressure will be 10 to 20 m from the surface to 60 km altitude. The errors described here are random such that climatological averages derived from this data should be significantly more accurate.

As we have shown, these levels of performance will be degraded only slightly (generally by less than a factor of 2) in the presence of clouds. The technique can accurately profile liquid water clouds and may be able to similarly profile ice clouds. These profiles will be horizontally averaged liquid water owing to the limb viewing geometry. The technique is therefore best suited for characterizing stratiform-type clouds. The along-track resolution is comparable to the 200 to 300 km of the GPS occultation observations but the shorter 22 and 183 GHz wavelengths improve the diffraction-limited vertical resolution to 100 to 300 m.

Figures 11a and b summarize and compare the vertical resolution and precision of BRIGHTOC and other present and planned satellite sensors. The figures indicate BRIGHTOC's combined dynamic range, accuracy, vertical resolution and ability to penetrate and characterize clouds extend significantly beyond that of other space-borne atmospheric sensors. Furthermore the BRIGHTOC retrieval is significantly simpler and more direct than passive retrievals because the source is a point source with known properties in contrast to the extended natural sources used in passive observations.

With regard to climate related applications, it is extremely important to note that in the BRIGHTOC technique a unique relation exists between the observables and the derived atmospheric variables. As such, unique retrievals can be generated *independent* of models unlike nadir-viewing passive sensors which must rely on background guesses from models or climatology to achieve unique retrievals. Therefore the BRIGHTOC observations are significantly better at characterizing the true signatures of underlying climatic processes and assessing the accuracy of climate models. A constellation of such sensors would provide an all-weather, global remote sensing capability including full sampling of the diurnal cycle for process studies related to water, and climate research and weather prediction in general.

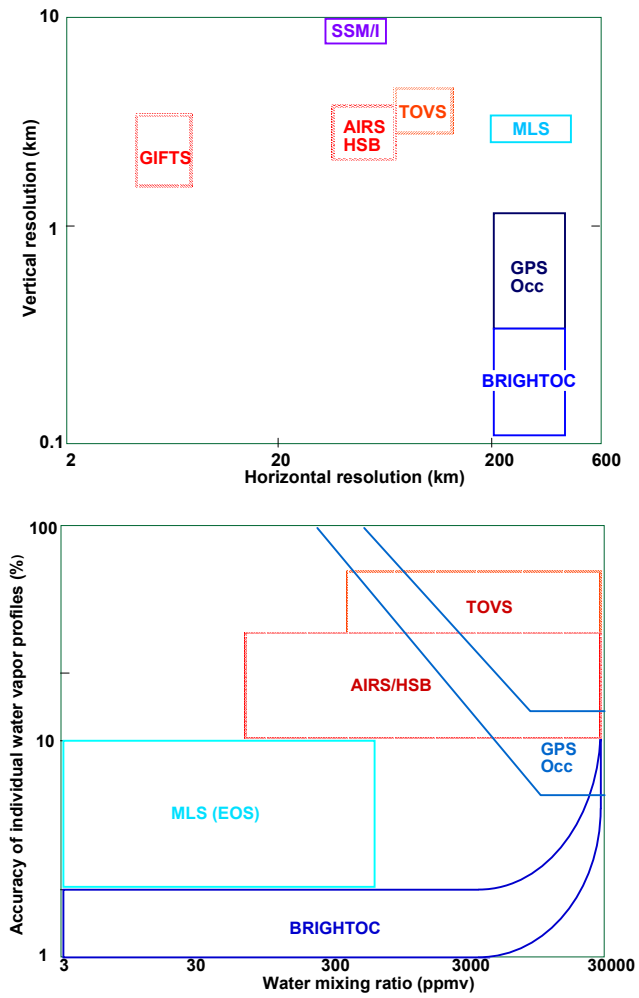

Figure 11: Comparison of BRIGHTOC performance with other existing and planned satellite sensors

VIII. References

Evans, K. F. and G. L. Stephens, Microwave radiative transfer through clouds composed of realistically shaped ice crystals, Part I: Single scattering properties, *JAS*, **52**, 2041- 2057, 1995.

Feng, D. D., S. Syndergaard, B. M. Herman, E. R. Kursinski, T. P. Yunck, and F. W. Romberg, 2001, Deriving atmospheric water vapor and ozone profiles from active microwave occultation measurements", in Sensors, Systems, and Next-Generation Satellites IV, edited by H. Fujisada, J. B. Lurie, A. Ropertz, and K. Weber, Vol. 4169 of SPIE Proceedings Series, pp. 299-308.

Fjeldbo, G., A. J. Kliore, and V. R. Eshleman, 1971, The neutral atmosphere of Venus as studied with the Mariner V radio occultation experiments, *Astron. J*., **76**, 123-140.

Healy S. B., and J. R. Eyre, 2000, Retrieving temperature, water vapour and surface pressure information from refractive-index profiles derived by radio occultation: A simulation study, *Q. J. R. Met. Soc*., **126**, 1661-1683.

Jenkins, J. M., P.G. Steffes, 1991, Results for 13-cm absorptivity and H2SO4 abundance profiles from the season-10 (1986) Pioneer Venus orbiter radio occultation experiment, *Icarus*, **90**, 129-138.

Jenkins, J. M., P.G. Steffes, D. P. Hinson, J. D. Twicken, and G. L.Tyler, 1994, Radio occultation studies of the Venus atmosphere with the Magellan spacecraft. 2. Results from the October 1991 experiments, *Icarus*, **110**, 79-94.

Kursinski, E.R., G.A. Hajj, K.R. Hardy, L.J. Romans and J.T. Schofield, 1995, Observing tropospheric water vapor by radio occultation using the Global Positioning System, *Geophys. Res. Lett*., **22**, 2365-2368.

Kursinski, E.R., et al., 1996, Initial Results of Radio Occultation Observations of Earth's Atmosphere Using the Global Positioning System, *Science*, **271**, 1107-1110.

Kursinski, E. R., G. A. Hajj, J. T. Schofield, R. P. Linfield and K. R. Hardy, Observing Earth's atmosphere with radio occultation measurements using the Global Positioning System, *J. Geophys. Res*., **102**, 23429-23465, 1997.

Kursinski, E. R., G. A. Hajj, S. S. Leroy and B. Herman, 2000a, The Radio Occultation Technique, *Terrestrial, Atmospheric and Oceanic Sciences*, **11**, 53-114.

Kursinski, E. R., S. B. Healy and L. J. Romans, 2000b, Initial Results of Combining GPS Occultations with ECMWF Global Analyses within a 1Dvar Framework, *Earth, Planets and Space*, **52**, 885-892.

Kursinski, E. R. and G. A. Hajj, 2001, A comparison of water vapor derived from GPS occultations and global weather analyses, *J. Geophys. Res.,* **106**, 1113-1138.

Kursinski et al., A microwave occultation observing system optimized to characterize atmospheric water, temperature and geopotential via absorption, *JTECH*, in press, 2002.

Lindal, G. F., G.E. Wood, G. S. Levy, J.D. Anderson, D. N. Sweetnam, H. B. Hotz, B. J. Buckles, D. P. Holmes, P. E. Doms, V. R. Eshleman, G. L. Tyler and T. A..Croft, 1981, The atmosphere of Jupiter: An analysis of the Voyager radio Occultation measurements*, J. Geophys. Res*., **86**, 8721-8727.

Poli, P., J. Joiner and E. R. Kursinski, 2002, 1DVar analysis of temperature and humidity using GPS radio occultation refractivity data, in press *J. Geophys. Res.*

Stevens, B., et al., 2002: Dynamics and Chemistry of Marine Stratocumulus -- DYCOMS-II. BAMS, submitted February 7, 2002.

Tricomi, F. G., *Integral Equations*, Dover, Mineola, N. Y., 1985.

Tyler G.L., et al., 1989, Voyager Radio Science Observations of Neptune and Triton, *Science*, **246**, 1466-1473.

Ware, R., et al., 1996, GPS sounding of the atmosphere from low Earth orbit - preliminary results, *Bull. Am. Meteorol. Soc.,* **77**, 19-40.

Zou, X., F. Vandenberge, B. Wang, et al., 1999, A ray-tracing operator and its adjoint for the use of GPS/MET refraction angle measurements, *J. Geophys. Res*., **104**, 22301-22318.